Biomedical Optics EXPRESS

Design and performance of an ultra-flexible two-photon microscope for in vivo research

Johannes M. Mayrhofer,[1,2] Florent Haiss,[1,2,3,4,5] Dominik Haenni,[6,7] Stefan Weber,[1] Marc Zuend,[1,2] Matthew J. P. Barrett,[1,2] Kim David Ferrari,[1,2] Philipp Maechler,[1,2] Aiman S. Saab,[1,2] Jillian L. Stobart,[1,2] Matthias T. Wyss,[1,2] Helge Johannssen,[1,2] Harald Osswald,[1] Lucy M. Palmer,[8,9] Vincent Revol,[10] Claus-Dieter Schuh,[7] Claus Urban,[10] Andrew Hall,[7] Matthew E. Larkum,[9] Edith Rutz-Innerhofer,[10] Hanns Ulrich Zeilhofer,[1,2] Urs Ziegler,[6] and Bruno Weber[1,2,*]

[1]*Institute of Pharmacology and Toxicology, University of Zurich, Winterthurerstrasse 190, 8057 Zürich, Switzerland*
[2]*Neuroscience Center Zurich, Winterthurerstrasse 190, 8057 Zurich, Switzerland*
[3]*IZKF Aachen, Medical Faculty of the RWTH Aachen University, Pauwelsstraße 30, 52074 Aachen, Germany*
[4]*Institute for Neuropathology, RWTH Aachen University, Pauwelsstraße 30, 52074 Aachen, Germany*
[5]*Department of Ophthalmology, RWTH Aachen University, Pauwelsstraße 30, 52074 Aachen, Germany*
[6]*Center for Microscopy and Image Analysis, University of Zurich, Winterthurerstrasse 190, 8057 Zurich, Switzerland*
[7]*Institute of Anatomy, University of Zurich, Winterthurerstrasse 190, 8057 Zurich, Switzerland*
[8]*Florey Instittue, University of Melbourne, 30 Royal Parade, Melbourne, Victoria, 3010, Australia*
[9]*Neuroscience Research Center, Charité-Universitätsmedizin Berlin, Charitéplatz 1, 10117 Berlin, Germany*
[10]*CSEM Suisse d'Electronique et de Microtechnique, Technoparkstrasse 1, 8005 Zurich, Switzerland*
[*]*bweber@pharma.uzh.ch*

Abstract: We present a cost-effective in vivo two-photon microscope with a highly flexible frontend for in vivo research. Our design ensures fast and reproducible access to the area of interest, including rotation of imaging plane, and maximizes space for auxiliary experimental equipment in the vicinity of the animal. Mechanical flexibility is achieved with large motorized linear stages that move the objective in the X, Y, and Z directions up to 130 mm. 360° rotation of the frontend (rotational freedom for one axis) is achieved with the combination of a motorized high precision bearing and gearing. Additionally, the modular design of the frontend, based on commercially available optomechanical parts, allows straightforward updates to future scanning technologies. The design exceeds the mobility of previous movable microscope designs while maintaining high optical performance.

OCIS codes: (000.1430) Biology and medicine; (180.4315) Nonlinear microscopy; (180.2520) Fluorescence microscopy; (120.4880) Optomechanics.

References and links

1. B. Weber and F. Helmchen, *Optical Imaging of Neocortical Dynamics* (New York: Springer, 2014).
2. W. Denk, J. H. Strickler, and W. W. Webb, "Two-photon laser scanning fluorescence microscopy," Science **248**(4951), 73–76 (1990).
3. F. Helmchen and W. Denk, "Deep tissue two-photon microscopy," Nat. Methods **2**(12), 932–940 (2005).
4. K. Svoboda and R. Yasuda, "Principles of two-photon excitation microscopy and its applications to neuroscience," Neuron **50**(6), 823–839 (2006).
5. A. M. Hall, C. Crawford, R. J. Unwin, M. R. Duchen, and C. M. Peppiatt-Wildman, "Multiphoton imaging of the functioning kidney," J. Am. Soc. Nephrol. **22**(7), 1297–1304 (2011).
6. A. M. Hall and B. A. Molitoris, "Dynamic multiphoton microscopy: focusing light on acute kidney injury," Physiology (Bethesda) **29**(5), 334–342 (2014).
7. C. Schuh, D. Haenni, E. Craigie, U. Ziegler, B. Weber, O. Devuyst, and A. Hall, "Intravital imaging of the kidney using long wavelength multiphoton excitation," in press.
8. D. Huber, D. A. Gutnisky, S. Peron, D. H. O'Connor, J. S. Wiegert, L. Tian, T. G. Oertner, L. L. Looger, and K. Svoboda, "Multiple dynamic representations in the motor cortex during sensorimotor learning," Nature **484**(7395), 473–478 (2012).
9. D. J. Margolis, H. Lütcke, K. Schulz, F. Haiss, B. Weber, S. Kügler, M. T. Hasan, and F. Helmchen, "Reorganization of cortical population activity imaged throughout long-term sensory deprivation," Nat. Neurosci. **15**(11), 1539–1546 (2012).

#242788 Received 10 Jun 2015; revised 28 Sep 2015; accepted 28 Sep 2015; published 2 Oct 2015

10. J. M. Mayrhofer, F. Haiss, F. Helmchen, and B. Weber, "Sparse, reliable, and long-term stable representation of periodic whisker deflections in the mouse barrel cortex," Neuroimage **115**, 52–63 (2015).
11. L. J. Gentet, M. Avermann, F. Matyas, J. F. Staiger, and C. C. H. Petersen, "Membrane Potential Dynamics of GABAergic Neurons in the Barrel Cortex of Behaving mice," Neuron **65**(3), 422–435 (2010).
12. L. J. Gentet, Y. Kremer, H. Taniguchi, Z. J. Huang, J. F. Staiger, and C. C. H. Petersen, "Unique functional properties of somatostatin-expressing GABAergic neurons in mouse barrel cortex," Nat. Neurosci. **15**(4), 607–612 (2012).
13. A. Holtmaat and K. Svoboda, "Experience-dependent structural synaptic plasticity in the mammalian brain," Nat. Rev. Neurosci. **10**(9), 647–658 (2009).
14. M. L. Andermann, "Chronic cellular imaging of mouse visual cortex during operant behavior and passive viewing," Front. Cellullar Neurosci., 2010.
15. D. A. Dombeck, A. N. Khabbaz, F. Collman, T. L. Adelman, and D. W. Tank, "Imaging Large-Scale Neural Activity with Cellular Resolution in Awake, Mobile Mice," Neuron **56**(1), 43–57 (2007).
16. J. M. Mayrhofer, V. Skreb, W. von der Behrens, S. Musall, B. Weber, and F. Haiss, "Novel two-alternative forced choice paradigm for bilateral vibrotactile whisker frequency discrimination in head-fixed mice and rats," J. Neurophysiol. **109**(1), 273–284 (2013).
17. D. H. O'Connor, N. G. Clack, D. Huber, T. Komiyama, E. W. Myers, and K. Svoboda, "Vibrissa-Based Object Localization in Head-Fixed Mice," J. Neurosci. **30**(5), 1947–1967 (2010).
18. S. Sachidhanandam, V. Sreenivasan, A. Kyriakatos, Y. Kremer, and C. C. H. Petersen, "Membrane potential correlates of sensory perception in mouse barrel cortex," Nat. Neurosci. **16**(11), 1671–1677 (2013).
19. C. Schwarz, H. Hentschke, S. Butovas, F. Haiss, M. C. Stüttgen, T. V. Gerdjikov, C. G. Bergner, and C. Waiblinger, "The head-fixed behaving rat--Procedures and pitfalls," Somatosens. Mot. Res. **27**(4), 131–148 (2010).
20. H. C. Johannssen and F. Helmchen, "In vivo Ca2+ imaging of dorsal horn neuronal populations in mouse spinal cord," J. Physiol. **588**(18), 3397–3402 (2010).
21. R. Prakash, O. Yizhar, B. Grewe, C. Ramakrishnan, N. Wang, I. Goshen, A. M. Packer, D. S. Peterka, R. Yuste, M. J. Schnitzer, and K. Deisseroth, "Two-photon optogenetic toolbox for fast inhibition, excitation and bistable modulation," Nat. Methods **9**(12), 1171–1179 (2012).
22. M. L. Andermann, N. B. Gilfoy, G. J. Goldey, R. N. S. Sachdev, M. Wölfel, D. A. McCormick, R. C. Reid, and M. J. Levene, "Chronic cellular imaging of entire cortical columns in awake mice using microprisms," Neuron **80**(4), 900–913 (2013).
23. T. A. Pologruto, B. L. Sabatini, and K. Svoboda, "ScanImage: flexible software for operating laser scanning microscopes," Biomed. Eng. Online **2**(1), 13 (2003).
24. A. San Martín, S. Ceballo, F. Baeza-Lehnert, R. Lerchundi, R. Valdebenito, Y. Contreras-Baeza, K. Alegría, and L. F. Barros, "Imaging Mitochondrial Flux in Single Cells with a Fret Sensor for Pyruvate," PLoS One **9**(1), e85780 (2014).
25. T. Euler, S. E. Hausselt, D. J. Margolis, T. Breuninger, X. Castell, P. B. Detwiler, and W. Denk, "Eyecup scope-optical recordings of light stimulus-evoked fluorescence signals in the retina," Pflüg. Arch. - Eur. J. Phys. **457**(6), 1393–1414 (2009).
26. D. D. Stettler, H. Yamahachi, W. Li, W. Denk, and C. D. Gilbert, "Axons and synaptic boutons are highly dynamic in adult visual cortex," Neuron **49**(6), 877–887 (2006).
27. D. Flickinger, V. Iyer, D. Huber, D. O'Connor, S. Peron, N. Clack, J. Chandrashekar, and K. Svoboda, "MIMMS: a modular, open design microscopy platform for in vivo imaging of neural tissues.," presented at the SfN 2010, 2010.
28. W. Göbel, J. N. D. Kerr, A. Nimmerjahn, and F. Helmchen, "Miniaturized two-photon microscope based on a flexible coherent fiber bundle and a gradient-index lens objective," Opt. Lett. **29**(21), 2521–2523 (2004).
29. J. Sawinski, D. J. Wallace, D. S. Greenberg, S. Grossmann, W. Denk, and J. N. D. Kerr, "Visually evoked activity in cortical cells imaged in freely moving animals," Proc. Natl. Acad. Sci. U.S.A. **106**(46), 19557–19562 (2009).
30. D. J. Wallace, D. S. Greenberg, J. Sawinski, S. Rulla, G. Notaro, and J. N. D. Kerr, "Rats maintain an overhead binocular field at the expense of constant fusion," Nature **498**(7452), 65–69 (2013).
31. B. F. Grewe, F. F. Voigt, M. van 't Hoff, and F. Helmchen, "Fast two-layer two-photon imaging of neuronal cell populations using an electrically tunable lens," Biomed. Opt. Express **2**(7), 2035–2046 (2011).

1. Introduction

High precision structural and functional images of the living brain have been a dream for neuroscientists for a long time. A wide range of optical methods have become indispensable for achieving this goal [1]. More than two decades ago, Denk and colleagues introduced two-photon laser scanning fluorescence microscopy (2PLSM) for biological applications [2]. Since then, considerable methodological progress has been made (see reviews [3, 4]) to the point where 2PLSM has become one of the most important in vivo techniques for the neurosciences. In addition, the importance for other organ systems continues to increase [5]. These experiments are facilitated with the use of dedicated in vivo two-photon instruments that differ significantly from standard upright microscopes. For example, two-photon imaging

#242788 Received 10 Jun 2015; revised 28 Sep 2015; accepted 28 Sep 2015; published 2 Oct 2015

in the kidney using the inverted approach leads to more stable conditions [6, 7]. Confining excitation to the focal volume, better tissue penetration and reduced phototoxicity out of the focal plane - due to the near infrared excitation through pulsed laser light - are the major advantages of 2PLSM over confocal fluorescent microscopy.

The use of 2PLSM in living organisms is particularly powerful when combined with genetically encoded fluorophores. For structural imaging, various fluorescent proteins have been developed, which allow chronic labelling and visualization of specific cell types over days, weeks or even months when combined with chronic imaging windows. Fluorescent molecules that are able to provide functional information are equally important tools. Calcium sensors are probably the most prominent example that enables the interrogation of activity on a cellular level and unsurpassed spatial resolution. The advent of genetic encoding added yet another level of importance to these indicators because many biological questions can only be addressed in a chronic, i.e. repeated measure, experimental setting. Today, numerous labs use genetically encoded sensors for calcium (GECIs) or for membrane potential (genetically-encoded voltage indicators (GEVIs)) routinely. Other genetically encoded indicators suitable for 2PLSM, for instance to measure metabolite concentrations, are emerging. Recent applications are recordings of activity from the same population of neurons over long time periods during motor learning, plasticity and stimulus stability [8–10], targeted electrophysiological recording of genetically identified neurons to understand circuit function [11, 12], as well as monitoring structure and activity changes on the dendrite level (reviewed in [13]).

Ultimately, to understand brain function, we need to causally link the activity of different genetically identified cell classes (or even subcellular compartments) and neuronal populations to specific behavioral tasks. The head fixed preparation, known for its well-controlled psychophysical conditions (stimulus delivery and response monitoring) in non-human primate studies, has been adapted to rodents by numerous groups [14–19]. Two-photon imaging of lateral cortical regions in awake, head-fixed animals poses a problem, since tilting the animal to adjust the imaging plane to be tangential to the cortical surface should be avoided. In acute preparations of the spinal cord, imaging the dorsal horn from an angle allows bypassing the incoming peripheral fiber tracts which in turn improves gray matter image quality significantly [20].

Our aim was to design a cost-effective two-photon microscope with a highly flexible frontend that ensures 1) fast and reproducible access to the area of interest, including rotation of the imaging plane; 2) maximized space for auxiliary experimental equipment in the immediate vicinity of the animal; and 3) high optomechanical adaptability warranting fast implementation of future technology, such as novel scan technology, detection hardware or two-photon optogenetics [21].

2. Methods and results

2.1 Mechanical design

High flexibility in terms of translation of the objective and space around the objective are advantageous for in vivo research. We use industry standard linear stages (with a length of 390 mm, LF 4 and LF 6; Isel, Germany) driven by stepper motors (2 phase step motor, SECM 268 - E 2.3 A, EC-Motion, Germany) which were stacked on each other using custom made black anodized aluminum parts, resulting in 130 mm of translation freedom of the objective in each of the X, Y, and Z directions (Fig. 1(A), 1(B)). The microscope frontend (FE in Fig. 1(A)) was designed such that there is 193 mm space behind the objective (Fig. 1(A), green bar) giving enough space to mount additional recording (e.g. motorized pipette holders) or stimulation devices (e.g. optical fiber for optogenetic stimulation).

Similar to many other biological structures, the cortex is curved in different axes. In addition, the cortex is a layered structure, in which the different layers are part of a complex information processing circuit. Orienting the imaging plane to be parallel (i.e. imaging many neurons from the same layer) or orthogonal to the cortical layers (i.e. obtaining a subset of

#242788 Received 10 Jun 2015; revised 28 Sep 2015; accepted 28 Sep 2015; published 2 Oct 2015

neurons from each layer [22]) can be essential for certain experimental questions. Here, the aim was to design the microscope mechanics in the way that the focal point of the objective matches the pivot point of the rotation axis (Fig. 1(C)). In this way, the orientation of the imaging plane can be easily adjusted without changing the depth of the region of interest in the center of the imaging field of view. A reliable and precise motorized rotation was established by using a combined high precision bearing and gearing (HFUS-25-160-2SH, Harmonic Drive, Germany) driven by a stepper motor (2 phase step motor, SECM 268 - E 2.3 B-BRK26, EC-Motion, Germany). The rotational freedom of the objective is 360 degrees (half of it is shown in Fig. 1(C)), which renders an inverted microscope position possible. For small and fast adjustments of the focal plane along the Z-direction, the objective was mounted to an additional piezo motor-driven linear stage with 800 μm travel range and a precision of 1.8 nm (P-628.1CD, Physik Instrumente, Germany).

Control signals for stepper motors were generated by a high performance 6 axis stepper/servo motion controller (NI PCI-7356, National Instruments, USA) and amplified (SMD276, EC-Motion, Germany). All axes were controlled by custom written LabVIEW software (National Instruments, USA), which also allowed gearing of X-axis with the Z-axis (Fig. 1(C)). X/Z gearing is required to move within the focal plane whenever the microscope is rotated.

The mechanical design (set of 3D CAD files in STP format),the motion control software (National Instruments Labview VI) and additional information can be obtained through the following weblink:

http://www.pharma.uzh.ch/research/functionalimaging/2pmicroscope.html.

#242788 Received 10 Jun 2015; revised 28 Sep 2015; accepted 28 Sep 2015; published 2 Oct 2015

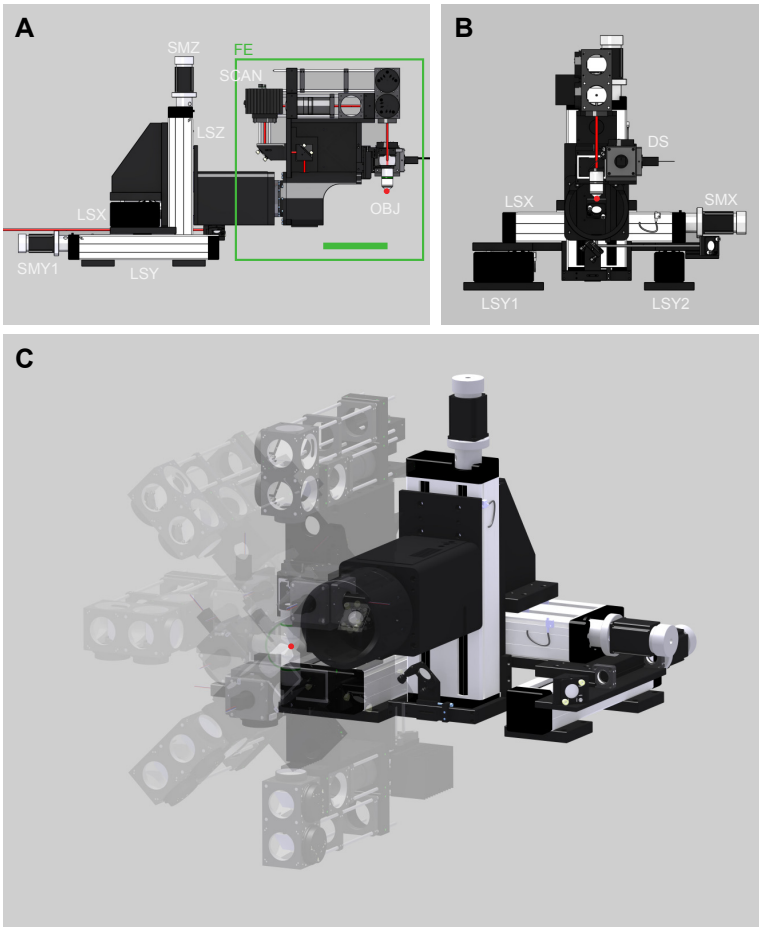

Fig. 1. Mechanical design. (A) Side view of the microscope. Green line indicates 193 mm space behind objective (OBJ). (B) Front view of the microscope. (C) 3D view showing the rotational freedom of microscope frontend (FE). Linear stage for X axis (LSX), linear stage one and two for Y axis (LSY1 and LSY2), linear stage for Z axis (LSZ), stepper motors (SMX, SMY1, SMY2, SMZ, SMR (not shown)), detection system (DS), objective (OBJ), and mounting block for scanners (SCAN). Focal point of OBJ is highlighted with a red dot.

2.2 Optical design

Each of the motor-driven linear axes carries one mirror (held by a commercially available kinematic mirror mount) mounted at an angle of 45° with respect to the translation direction. Each mirror deflects the laser beam to the mirror on the next axis (see MX and MY in Fig. 2(A)). The laser beam is then deflected onto a mirror located on the Z-axis (MZ in Fig. 2(A)), which directs the beam through a hollow shaft onto the rotation axis mirror (MR1 in Fig. 2(A)). Two additional mirrors (see MR2 and MR3 in Fig. 2(A)) were used to steer the laser beam to the desired central position of the galvanometric scan mirrors (SCAN in Fig. 2). This design allows translation and rotation of the microscope head while maintaining a stable beam position with respect to the galvanometric scanners (SCAN in Fig. 2(A), 6215H; Cambridge Technology, USA), scan lens (SL in Fig. 2, 75 mm focal length: AC508-075-B, Thorlabs, USA), tube lenses (TL1 and TL2 in Fig. 2, 300 mm and 400 mm focal length: AC508-300-B and AC508-400-B, Thorlabs, USA), the water immersion microscope objective (OBJ in Fig. 2, W-Plan Apochromat 20x/1.0 DIC, Zeiss, Germany) as well as the detection system (DS in Fig. 2(A)). An exactly parallel alignment of the laser beam to the linear axis directions, as well as an alignment of the beam to the rotational axis are essential and ensure that translating

#242788 Received 10 Jun 2015; revised 28 Sep 2015; accepted 28 Sep 2015; published 2 Oct 2015

and rotating the microscope does not affect the position of the laser beam (indicated by the red line in Fig. 2(A)) relative to the scan mirrors. The mounting block of the scanners as wells as the scan and tube lenses are attached on a two inch cage system for simple adjustment of distances between the optical components, alignment with the laser beam and future extensibility (Fig. 1). To reach large fields of view 2" optical components are used (Fig. 2(B)). The optics are designed to obtain an overfilling of the back aperture of large numerical aperture (NA) objectives to improve spatial resolution [3].

For efficient detection of the emission light (ballistic and scattered light) the detection system, made up of two photo multiplier modules (PMMs), was positioned as close as possible to the back aperture of objective by mounting the dichroic beam-splitter (DBS1 in Fig. 2(B): G380255036, Linos, Germany) immediately after the objective back aperture and using a collection lens with a short focal length (CL in Fig. 2(B), 60 mm focal length: ACL5040-A, Thorlabs, USA). The collection lens has large clear aperture (2") to maximize collection of scattered light. Emission was detected with two gallium arsenide phosphide (GaAsP) detector modules (PMM1 and PMM2 in Fig. 2(B), H10770PA-40; Hamamatsu Photonics, Japan). Signals were pre-amplified before digitization (Sigmann Elektronik, Germany). For testing the optical performance, the following filters were used (Semrock, USA): dichroic beam-splitter 515 DCXR (DBS2 in Fig. 2(B)), band-pass filter BrightLine HC 542/50 (yellow channel) and band-pass filter BrightLine HC 475/64 (blue channel). In addition, each channel was equipped with a short pass filter (HC 770/SP, Semrock, USA) for blocking infra-red light.

In order to project the imaging plane to a wide-field camera for coarse positioning of the imaging field of view at the beginning of an experiment, the dichroic beam-splitter (DBS1 in Fig. 2(B)) can be slid out from the optical path and precisely repositioned (NDN 1-50.40, Schneeberger Linear Technology, Switzerland). When slid out, visible light can pass the dichroic beam-splitter (DBS3 in Fig. 2: NT43-957, Edmund Optics, Germany) placed between lens TL2 and lens TL1 and is finally deflected by a silver mirror (CPM in Fig. 2) to the camera path (not shown; 180 mm focal length lens, objective and low budget CMOS sensor camera).

Fluorophores are excited with a Ti:sapphire laser (680 - 1300 nm, 120 fs pulses at 80 MHz, Insight Dual Deep See, Newport Spectra-Physics, CA, USA). Laser intensity is modulated with a Pockels Cell (KD*P 350, model 350-80LA, and driver electronics model 302 RM, Conoptics, USA). The first beam expansion step and divergence compensation of the laser beam is done with the use of a telescope (expansion factor depending on the objective used, 1.5x in the case of the W-Plan Apochromat 20x/1.0 DIC, Zeiss, Germany).

Image acquisition is controlled by the Matlab software ScanImage [23] running on a personal computer equipped with multifunctional data acquisition cards (National Instruments, USA).

The total cost of the microscope lies around 70'000 € (without laser, Pockels cell and microscope objective), which compares very well to other commercially available two-photon microscopes with similar features.

#242788 Received 10 Jun 2015; revised 28 Sep 2015; accepted 28 Sep 2015; published 2 Oct 2015

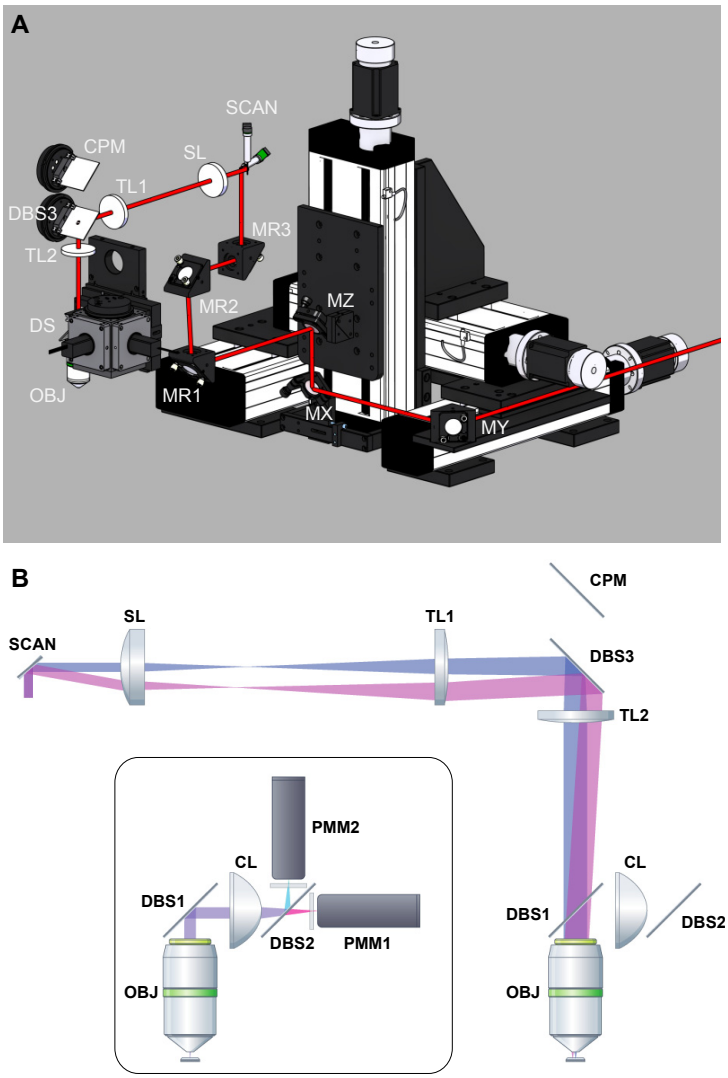

Fig. 2. Optical design. (A) Position of optical components of the microscope. Mirror on the X, Y, Z, and rotation axes (MX, MY, MZ, MR1), additional mirrors on microscope head (MR2 and MR3), galvanometric scanner (SCAN), scan lens (SL), tube lenses (TL1 and TL2), dichroic beam splitter (DBS3), camera path mirror (CPM), detection system (DS), and objective (OBJ) (B) optical path of the scan optics and detection path (inset). Labels as in (A), but only X scan mirror of galvo scanners (SCAN) is shown, as well as dichroic beam-splitters (DBS1 and DBS2), condenser lens (CL), dichroic beam-splitter for emission (DBS2), dichroic beam-splitter for camera path (DBS3), and photo multiplier modules (PMM1 and PMM2).

2.3 Constant resolution over entire travel range and mechanical stability

To assess the mechanical stability and optical performance of the microscope we measured the point spread function (PSF) at different positions and rotational angles of the frontend using fluorescent microspheres (PS-Speck green (505/515), 170 nm diameter, lifetechnologies, P-7220). Before the first experiment, the collar ring of the microscope objective (Olympus XLPLan N, 25x, 1.05) was iteratively adjusted for optimal imaging performance. The microspheres were placed on a conventional microscope slide and embedded in the provided mounting medium (lifetechnologies, P-7220). The sample was sealed using a 0.17 mm cover glass and nail polish. To avoid imaging far off the optical axis,

#242788 Received 10 Jun 2015; revised 28 Sep 2015; accepted 28 Sep 2015; published 2 Oct 2015

microspheres were chosen in the center of the FOV. The fluorescent microspheres were excited at a wavelength of 1000 nm with a laser power of 10 mW (measured after the objective). Z-stacks (90 slices) were recorded with a lateral resolution of 512x512 pixels (45.7 nm/pixel) and a Z-increment of 250 nm. The pixel integration time was 3.9 µs (leading to a frame rate of 0.98 Hz). The stepper motors controlling the large movements of the microscope frontend were deactivated during the measurements to avoid residual vibrations. X, Y and Z profiles of the measured point spread functions were extracted using ImageJ (U. S. National Institutes of Health, USA): The profiles were extracted along the main axes of the PSF, which were located by taking the slices with the smallest extension of the PSF and finding its highest intensity pixel. The data was exported and further analyzed using OriginPro (OriginPro 9.1.0, OriginLab Corporation, USA). The profiles were fitted to a Gaussian function using a Levenberg Marquardt algorithm. At the center position (Y-position 65 mm, X-position 65 mm, Rotation 0 degrees), we measured a PSF (FWHM) of 539 nm (X), 491 nm (Y) and 1613 nm (Z). Between the different microscope frontend positions (0 – 130 mm for X and Y and 0 – 180 degrees for the rotation) the PSF remained within 9.2% (X), 3.3% (Y) and 12.7% (Z) of the respective mean FWHM. The consistent FWHM values across the different microscope frontend positions confirm the robustness of the mechanical design and the constant optical performance of the microscope design over its entire operation range.

The mechanical stability was assessed by measuring drift over long time spans with a highly accurate laser triangulation displacement sensor (max. resolution 0.03 µm; Micro-Epsilon ILD2300-10, Germany). We found that the relative drift between the the objective and the optical table stayed below 1 µm per hour in all directions. Since the microscope was designed to be used with awake, behaving animals, their movement could induce vibrations on the cantilevered frontend through the optical table and by that create motion artifacts in the images. We tried to mimic this situation in a well controlled way by mechanically exiting the table. We placed a large voice coil on the optical table loaded with a 200 g mass, and moved this with amplitude of approx. 3 mm and a frequency between 0 and 50 Hz. At the same time, we imaged a grain of pollen at approx. 6 Hz. At almost all of the frequencies we did not observe any significant motion in the images; however, the system appeared to have a resonant frequency at approx. 20 Hz. Given that vibration/motion artefacts from an animal are unlikely to be so large or so perfectly periodic, we believe the microscope system is sufficiently resistant to vibration and is suitable for awake imaging. Our own practical experience with awake imaging clearly confirms this, as we have never encountered any issues with vibrations.

2.4 Re-positioning accuracy in the in vivo situation

To demonstrate the capabilities of the microscope for in vivo imaging, adeno-associated virus (AAV) carrying the pyruvate FRET nanosensor Pyronic [24] (AAV6 under human synapsin promoter or AAV9 under GFAP) injected mouse was implanted with a chronic window [9], [10]. The mouse was anesthetized with a mixture of fentanyl (0.05 mg per kg bodyweight; Sintenyl, Sintetica, Switzerland), midazolam (5 mg per kg bodyweight; Dormicum, Roche) and medetomidine (0.5 mg per kg bodyweight; Domitor, Orion Pharma) intraperitoneally. Volatile anesthetics were avoided to reduce brain swelling. The mouse was kept at 37°C with a temperature controlled head-system (Harvard Apparatus, USA). Surgical and experimental procedures were approved by the local veterinary authorities, conforming to the guidelines of the Swiss Animal Protection Law, Veterinary Office, Canton Zürich (Act of Animal Protection 16 December 2005 and Animal Protection Ordinance 23 April 2008).

In order to mimic consecutive imaging sessions (e.g. as in chronic imaging), we moved the microscope into its home position and then to a field of view (FOV). To assess accuracy within an imaging session, we subsequently moved the microscope between two alternating FOVs. Once a FOV was chosen, z-stacks were acquired covering the FOV (30 slices with a steps size of 1 µm) for offline image registration. Movement to the FOV was entirely controlled by entering co-ordinates into the motion software, yielding a measure of repositioning precision. Our protocol consisted of 10 repetitions for accessing the first FOV

#242788 Received 10 Jun 2015; revised 28 Sep 2015; accepted 28 Sep 2015; published 2 Oct 2015

from the home position of the microscope, and 12 repetitions for alternating between FOVs (Fig. 3). The repositioning accuracy was determined by image correlation analysis with custom Matlab software. Moving from the home position of the microscope to FOV1a (i.e. the inter-session protocol), the repositioning accuracy was $|\Delta x'| = 1.0 \pm 0.8$ µm, $|\Delta y'| = 2.0 \pm 1.5$ µm and $|\Delta z'| = 3.9 \pm 3.2$ µm (mean ± SD, Fig. 3(B), left part). The repositioning accuracy between FOVs (i.e. intra- session FOV switching) was $|\Delta x'| = 2.2 \pm 1.6$ µm, $|\Delta y'| = 1.3 \pm 1.1$ µm, and $|\Delta z'| = 3.7 \pm 3.9$ µm for FOV1b and $|\Delta x'| = 4.5 \pm 3.1$ µm, $|\Delta y'| = 1.7 \pm 1.5$ µm, and $|\Delta z'| = 6.3 \pm 6.3$ µm for FOV2 (Fig. 3(C)). Taken together, the repositioning precision of the presented microscope is in the order of 3 µm, allowing for repeated in vivo access of the same FOV of over many experimental days, even when the microscope has been used for a different set of experiments.

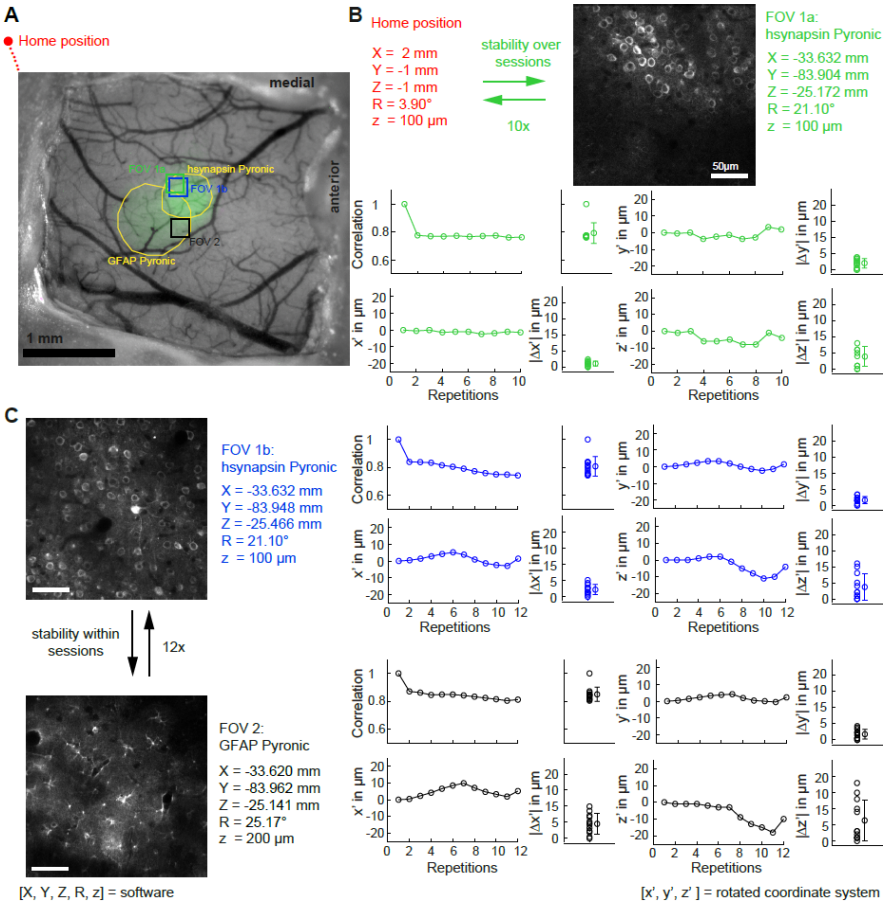

Fig. 3. Repositioning accuracy in the in vivo situation. (A) Wide field image of chronic window overlaid with indicator expression (green channel; hsynapsin-Pyronic and GFAP-Pyronic). (B) Schematic of the protocol used to measure the accuracy when repositioning the microscope in the same FOV over different sessions (upper panel). Shifts (x', y' and z') and absolute differences ($|\Delta x'|$, $|\Delta y'|$ and $|\Delta z'|$) between the initial FOV and subsequent repositioning in the same FOV. (C) Schematic of the protocol used to measure the repositioning accuracy between two FOVs within the same session (left panel). Differences between the initial FOVs and subsequent repositioning in the same FOV (nomenclature same as in (B)).

3. Discussion

The use of in vivo two-photon imaging has spread rapidly throughout the life sciences. The need for highly versatile and flexible setups has become particularly evident for neuroscience,

#242788 Received 10 Jun 2015; revised 28 Sep 2015; accepted 28 Sep 2015; published 2 Oct 2015

where experiments have become increasingly complex. Many investigations require a multimodal approach (e.g. combining electrophysiology, pharmacology and two-photon imaging) or have to be performed in awake behaving animals. These experiments are facilitated with the use of dedicated in vivo two-photon instruments that differ significantly from standard upright microscopes.

We have developed a cost effective, ultra-flexible two-photon microscope dedicated for in vivo imaging. The travel range of the X, Y, and Z translation of the objective's focal point reaches 130 mm in each direction, and the rotational freedom of the microscope is 360° for one axis. Despite this enormous flexibility, the microscope delivers excellent mechanical stability and optical performance.

3.1 Other moveable microscope designs

One of the first moveable microscope was developed by Denk and colleagues [25, 26]. The design allowed movement of the objective in three dimensions and manual rotation around one axis in order to reach more lateral parts of the brain. This design inspired the development of the now commercially available Moveable Objective Microscope (MOM) from Sutter instruments, which has travel range of 22 mm and one non-motorized rotational axis (0-180°, can be used in upright and inverted position). Here the scanning system does not rotate around the focal point, and this can make the alignment of additional experimental equipement e.g. pipettes difficult. The MOM has also been adjusted by other groups to increase its translational capabilities [27]. To our knowledge the most flexible microscope on the market is the Thorlabs Bergamo II Series. This microscope provides rotational freedom of 100° and translational freedom of 127 mm. Other companies offering two-photon microscopes have a higher starting price and inferior flexibility which make them less attractive for in-vivo research. A completely different approach is to miniaturize the two-photon microscope and mount it on the animal's head. Although there has been progress in this direction, such microscopes are mostly used in rats [28, 29]. Other drawbacks are the inferior optical performance and the difficulty in decoding naturalistic sensory stimuli without the head fixed preparation. However, to tackle certain scientific questions, freely moving animals are mandatory [30].

3.2 Outlook

Since the mechanical chassis was designed such that commercial optics and optomechnical components can be easily integrated, high flexibility for future developments is guaranteed. For example, it is possible to increase flexibility on the detection side by using fiber optics to detach the filters and detectors from the microscope. This would allow a larger number of channels or placing a shutter in front of the detectors during optogenetic light stimulation (e.g. with blue light).

For imaging in the awake state, motion artifacts can be a significant problem. Slow scan speeds (10 Hz frame rate) lead to in-frame distortions [15]. Therefore, for imaging in the awake animal it is advantageous to image with frame rates of about 30 Hz. This can be reached by using a resonance scanner for one scan direction. The design of the presented microscope makes it relatively simple to implement resonance scanning. Furthermore, an electrical tunable lens (TLS) could be placed in the excitation path of the microscope for fast volumetric scanning [31].

Another reasonably straightforward addition would be an extra galvanometric scanner system. An independent second infrared beam would allow imaging and specific two-photon based optogenetic stimulation of defined subpopulations in parallel [21].

Acknowledgments

The project was in part sponsored by the Swiss National Science Foundation and by the Hartmann Müller-Stiftung. BW and AH are members of the Clinical Research Priority Program "Molecular Imaging Network Zurich".